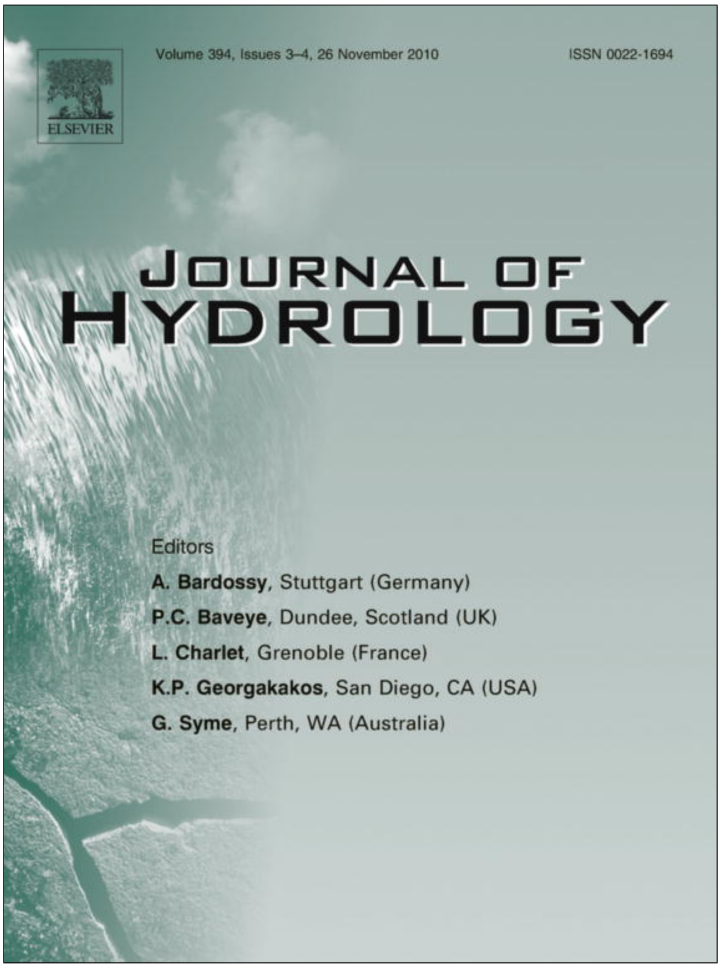
Volume 394, Issues 3–4, 26 November 2010
ISSN 0022-1694
ELSEVIER
JOURNAL OF
HYDROLOGY
Editors
A. Bardossy, Stuttgart (Germany)
P.C. Baveye, Dundee, Scotland (UK)
L. Charlet, Grenoble (France)
K.P. Georgakakos, San Diego, CA (USA)
G. Syme, Perth, WA (Australia)

Journal of Hydrology 394 (2010) 315–323

Contents lists available at ScienceDirect

Journal of Hydrology

journal homepage: www.elsevier.com/locate/jhydrol

A finite-element algorithm for modeling variably saturated flows

Mengxi Wu *

Institute of Mechanics, Chinese Academy of Sciences, Bei Si Huan Xi Road No.15, Beijing, PR China

ARTICLE INFO

Article history:
Received 7 April 2010
Received in revised form 12 July 2010
Accepted 5 September 2010

This manuscript was handled by Geoff Syme, Editor-in-Chief

Keywords:
Richards' equation
Variably saturated flow
Finite element method
Transient water table
Infiltration

SUMMARY

A general numerical algorithm in the context of finite element scheme is developed to solve Richards' equation, in which a mass-conservative, modified head based scheme (MHB) is proposed to approximate the governing equation, and mass-lumping techniques are used to keep the numerical simulation stable. The MHB scheme is compared with the modified Picard iteration scheme (MPI) in a ponding infiltration example. Although the MHB scheme is a little inferior to the MPI scheme in respect of mass balance, it is superior in convergence character and simplicity. Fully implicit, explicit and geometric average conductivity methods are performed and compared, the first one is superior in simulation accuracy and can use large time-step size, but the others are superior in iteration efficiency. The algorithm works well over a wide variety of problems, such as infiltration fronts, steady-state and transient water tables, and transient seepage faces, as demonstrated by its performance against published experimental data. The algorithm is presented in sufficient detail to facilitate its implementation.

1. Introduction

The standard approach to model variably saturated flow is using numerical methods to solve Richards' equation (RE). Most common approaches used finite difference or finite element spatial approximations with low order time integration schemes to solve Richards' equation, which are usually expressed in three standard forms: pressure head based, moisture content based and mixed-form where both variables are employed. The pressure based form can be adopted to deal with both saturation and un-saturation cases. However, for highly non-linear problems, such as infiltration into very dry soils, these methods may suffer from mass-balance error, convergence problems and poor iterative efficiency (Celia et al., 1990; Mcbride et al., 2005). The reason of poor mass balance resides in the time derivative term (Celia et al., 1990). While the derivatives of the moisture content ($\partial\theta/\partial t$) and $\partial\theta/\partial\psi \cdot \partial\psi/\partial t$ (θ = moisture content, ψ = pore pressure head, and t = time) are mathematically equivalent in the continuous partial differential equation, their discrete counterparts are not, and the nonequivalence of the discrete form is exacerbated by the highly non-linear nature of $\partial\theta/\partial\psi$. This leads to serious problems of mass-balance error and the error grows with the time-step size. Milly (1985) presented a mass-conservative numerical scheme in which a specific soil moisture capacity value (C) averaged over each element during each time-steps was used. This approach, coupled with mass-lumping (Neuman, 1999), ensures effectively global mass balance in the pressure head based equation. As for the moisture content based form, perfectly mass-conservative discrete approximations can be applied, but this form degenerates under fully saturated conditions, since a pressure–saturation relationship no longer exists. It cannot also be adopted to simulate layered soils since the moisture content is discontinuous across the contact face of different soils. A numerical technique for approximating the mixed-form equation has been developed to minimize the mass-balance errors and enhance computational efficiency. E.g. Celia et al. (1990) proposed a modified Picard iteration scheme that ensures mass balance by directly evaluating the moisture content change in a time-step from the change of the water pressure head, which was shown to provide excellent mass balance in modeling unsaturated problems with sharp wetting fronts. The mass-balance error problem reported by some other researchers (Kavetski et al., 2001; Hao et al., 2005) in applying this method to free drainage problems arose actually from the error in calculating the unsaturated boundary flow flux, and the error decreased rapidly when a smaller iteration tolerance was employed. A new convergence criterion was introduced in the modified Picard iteration method and was found to be computationally more efficient (Huang et al., 1996). However, the use of mass-conservative methods does not guarantee an accurate solution, and thus the main purpose of the present paper is to provide a general, mass-conservative and computationally efficient multi-dimensional finite element algorithm.

* Tel.: +86 10 82544191.
E-mail address: Wumx@imech.ac.cn

0022-1694/$ - see front matter © 2010 Elsevier B.V. All rights reserved.
doi:10.1016/j.jhydrol.2010.09.004

2. Basic equations

Water flowing through porous media is described by the Darcy equation written in the form

$$q_i = -h_{,j}k_r(\psi)K_{ij} = -K_{ij}k_r(\psi)(\psi+z)_{,j} \tag{1}$$

According to the mass-conservative principle and Eq. (1), Richards' equation (1931) governs saturated–unsaturated flows in porous media and can be deduced as

$$\frac{\partial\theta(\psi)}{\partial t} - [K_{ij}k_r(\psi)(\psi+z)_{,j}]_{,i} = Q \tag{2}$$

In Eqs. (1) and (2), q is the Darcy flux vector, $k_r(\psi)$is the relative hydraulic conductivity, K is the tensor of permeability for saturated media, $h = \psi + z$ is the hydraulic head, ψ is the pressure head, z is elevation above a reference datum, θ is the moisture content and Q is the source/sink term. The subscript $i,j = 1,\ldots,D$ are spatial indices of the Cartesian coordinates, D denotes the number of spatial dimension (2 or 3) and the summation convention is used for repeated indices.

Van Genuchten's (1980) (VG) equation for the soil water retention curve and Mualem's (1976) unsaturated relative permeability function are used to describe the soil properties.

$$\theta(\psi) = \begin{cases} \theta_r + (\theta_s - \theta_r)(1+|\alpha\psi|^n)^{-m}, & \psi < 0 \\ \theta_s, & \psi \geqslant 0 \end{cases} \tag{3}$$

$$k_r(s_e) = s_e^{1/2}\left[1-\left(1-s_e^{1/m}\right)^m\right]^2 \tag{4}$$

in which s_e is the effective saturation

$$s_e(\psi) = \frac{\theta(\psi)-\theta_r}{\theta_s-\theta_r} \tag{5}$$

In these equations, θ_r and θ_s are the residual and saturated moisture contents respectively, α and n are shape parameters, and $m = 1 - 1/n$.

3. Finite element formulation

Let Ω denotes the spatial domain, $\Omega \subset R^D$, where D is the spatial dimensionality. Let L denotes the boundary of ς. For any function v, the weak form of the mass balance Eq. (2) can be written as

$$\int_\Omega \left\{-[(\psi+z)_{,j}k_r(\psi)K_{ij}]_{,i} + C\frac{\partial\psi}{\partial t} - Q\right\} v d\Omega = 0 \tag{5}$$

where $C = \partial\theta/\partial\psi$ is the specific moisture capacity.

Since $(uv)_{,i} = u_{,i}v + uv_{,i}$, namely, $-u_{,i}\ v = uv_{,i} - (uv)_{,i}$, u represents $(\psi + z)_{,j}k_r\ (\psi)K_{ij}$ in Eq. (5), the above equation can be stated as

$$\int_\Omega (\psi+z)_{,j}k_r(\psi)K_{ij}v_{,i}d\Omega - \int_\Omega [(\psi+z)_{,j}k_r(\psi)K_{ij}v]_{,i}d\Omega + \int_\Omega \left[C\frac{\partial\psi}{\partial t} - Q\right] v d\Omega = 0 \tag{6}$$

According to the divergence theorem, the outward flux of a vector field through a closed surface is equal to the volume integral of the divergence of the region inside the surface, the second term in Eq. (6) can be transformed into $-\oint_L[(\psi+z)_{,j}k_r(\psi)K_{ij}v]n_i dL$, where L denotes the boundary surface of ς,n_i is the unit outward normal vector at the boundary surface, $q_n = -(\psi + z)_{,j}k_r(\psi)K_{ij}n_i$, is the flux vector at the boundary. Eq. (6) can be stated as

$$\int_\Omega (\psi+z)_{,j}k_r(\psi)K_{ij}v_{,i}d\Omega + \int_\Omega C\frac{\partial\psi}{\partial t}vd\Omega = \oint_L -q_n v dL + \int_\Omega Q v d\Omega \tag{7}$$

In the finite element context a spatial semi-discretization ς^h of the continuum domain ς is achieved by such union of a set of non-overlapping sub-domains ς_e (the finite elements) as

$$\Omega \approx \Omega^h = \bigcup_e \Omega_e \tag{8}$$

On any finite-element domain ς_e, the unknown variables and dependent coefficients are replaced by a continuous approximation that space and time are assumed separable. Thus $\psi = N_I\psi_I$, $z = N_I z_I$, $v = N_I v_I$, where N_I is the nodal basis shape function of an element and I is the serial number of a node in the element. Eq. (8) can be written as

$$\sum_e \int_{\Omega_e} (\psi+z)_J k_r(\psi)K_{ij}N_{J,j}N_{I,i}v_I d\Omega + \sum_e \int_{\Omega_e} CN_J\frac{\partial\psi_J}{\partial t}N_I v_I d\Omega = \oint_L -q_n N_I v_I dL + \sum_e \int_{\Omega_e} QN_I v_I d\Omega \tag{9}$$

The above equation is exact for any $[v_1, v_2, \ldots, v_I]$, so we can express the equation as

$$\sum_e \int_{\Omega_e} N_{I,i}k_r(\psi)K_{ij}N_{J,j}d\Omega\cdot(\psi+z)_J + \sum_e \int_{\Omega_e} CN_I N_J d\Omega\cdot\frac{\partial\psi_J}{\partial t} = \oint_L -q_n N_I dL + \sum_e \int_{\Omega_e} QN_I d\Omega \tag{10}$$

The second term in the above equation is a consistent form of time matrix which is also called mass matrix. Diagonalization of this term (mass-lumping) is important to avoid numerical oscillation which may occur ahead of the moisture front in infiltration problems (Celia et al., 1990; Neuman, 1999). Hence, Eq. (10) can be changed to

$$\sum_e \int_{\Omega_e} N_{I,i}k_r(\psi)K_{ij}N_{J,j}d\Omega\cdot(\psi+z)_J + \sum_e \int_{\Omega_e} C\frac{1}{l}\delta_{IJ}d\Omega\cdot\frac{\partial\psi_J}{\partial t} = \oint_L -q_n N_I dL + \sum_e \int_{\Omega_e} QN_I d\Omega \tag{11}$$

where l is the number of nodes in an element, δ_{IJ} is the Kronecker delta.

Eq. (11) is a multi-dimensional finite element discretization of the Richards' equation.

4. Temporal discretization

Temporal discretization of Eq. (2) with the fully implicit Picard method and a backward Euler method may be written as

$$\frac{\theta^{n,m}-\theta^{n-1}}{\Delta t} - [K_{ij}k_r^{n,m-1}(\psi^{n,m}+z)_{,j}]_{,i} = Q \tag{12}$$

where n denotes the time level, m identifies iteration level, θ is the moisture content, ψ^n denotes the approximate value of ψ at the nth discrete time level ($t = t^n$), $\Delta t = t^n - t^{n-1}$ is the time-step size, k_r^n denotes the relative hydraulic conductivity evaluated using ψ^n, and the solution is assumed to be known both at time level $n - 1$ and at iteration level $m - 1$. The expansion of $\theta^{n,m}$ by Celia et al. is expressed as

$$\theta^{n,m} = \theta^{n,m-1} + \left.\frac{\partial\theta}{\partial\psi}\right|^{n,m-1}(\psi^{n,m}-\psi^{n,m-1}) + 0(\delta^2) \tag{13}$$

If all the terms higher than the linear are neglected in Eq. (13) and the approximate equation is substituted into Eq. (12), we obtain

$$\frac{1}{\Delta t}C^{n,m-1}(\psi^{n,m}-\psi^{n,m-1}) + \frac{\theta^{n,m-1}-\theta^{n-1}}{\Delta t} - [K_{ij}k_r^{n,m-1}(\psi^{n,m}+z)_{,j}]_{,i} = Q \tag{14}$$

This mixed-form equation is named as the modified Picard iteration (Celia et al., 1990). It is inherently mass-conservative and has been widely used. The conjunction of (14) with finite element discretization Eq. (11) is expressed as

$$\sum_e \int_{\Omega_e} N_{I,i} K_{ij} N_{J,j} k_r(\psi^{n,m-1}) d\Omega \cdot (\psi^{n,m} + z)_J + \sum_e \int_{\Omega_e} \frac{C(\psi^{n,m-1})}{\Delta t} \times \frac{1}{l} \delta_{IJ} d\Omega \cdot \psi_J^{n,m} = \oint_L -q_n N_I dL + \sum_e \int_{\Omega_e} Q N_I d\Omega + \sum_e \int_{\Omega_e} \frac{C(\psi^{n,m-1})}{\Delta t} \frac{1}{l} \delta_{IJ} d\Omega \cdot \psi_J^{n,m-1} - \sum_e \int_{\Omega_e} \frac{1}{l} \delta_{IJ} \frac{\theta_J^{n,m-1} - \theta_J^{n-1}}{\Delta t} d\Omega \quad (15)$$

This is a fully implicit modified Picard iteration approximation of multi-dimensional problems in the context of finite element method.

As pointed out by Milly (1985), a mass-conservative solution may also be obtained with the head based formulation if the capacity term is evaluated in an appropriate manner (Huang et al., 1994). A modified head based formulation (Wu and Gao, 1999) is an alternative mass conservative scheme approximating Eq. (2), which is stated as

$$\overline{C}(\psi^n) \frac{\beta(\psi^n)\psi^n - \beta(\psi^{n-1})\psi^{n-1}}{\Delta t} - [K_{ij} k_r^n (\psi^n + z)_{,j}]_{,i} = Q \quad (16)$$

where $\overline{C}(\psi^n)$ is the chord value of the specific moisture capacity over the unsaturated pressure head domain $[\psi^{n-1}, \min(0, \psi^n)]$ or $[\psi^n, \min(0, \psi^{n-1})]$, β is a simple function as follows

$$\beta(\psi) = \begin{cases} 1, & \psi < 0 \\ 0, & \psi \geqslant 0 \end{cases} \quad (17)$$

$$\overline{C}(\psi^n) = \begin{cases} \frac{\theta(\psi^n) - \theta(\psi^{n-1})}{\beta(\psi^n)\cdot\psi^n - \beta(\psi^{n-1})\cdot\psi^{n-1}}, & |\beta(\psi^n)\cdot\psi^n - \beta(\psi^{n-1})\cdot\psi^{n-1}| \geqslant 0.01 \\ \frac{\theta(\psi^n) - \theta(\psi^n - 0.01)}{0.01}, & |\beta(\psi^n)\cdot\psi^n - \beta(\psi^{n-1})\cdot\psi^{n-1}| < 0.01 \end{cases} \quad (18)$$

The calculation domain of the specific moisture capacity is limited within the minus pressure head range, rather than involves positive pressure both in the temporal and the spatial domains.

Eq. (16) can also be written as

$$\frac{\overline{C}(\psi^n)}{\Delta t} \beta(\psi^n)\psi^n - [K_{ij} k_r^n (\psi^n + z)_{,j}]_{,i} = \frac{\overline{C}(\psi^n)}{\Delta t} \beta(\psi^{n-1})\psi^{n-1} + Q \quad (19)$$

Standard iteration techniques, such as Picard and Newton methods, can be used to solve Eq. (19) in combination with a spatial discretization method. The spatial discretization can be difference approximation or finite element approximation. Incorporating Eq. (19) into finite element discretization Eq. (11), we obtain

$$\sum_e \int_{\Omega_e} N_{I,i} K_{ij} N_{J,j} k_r(\psi^n) d\Omega \cdot (\psi^n + z)_J + \sum_e \int_{\Omega_e} \frac{\overline{C}(\psi^n)}{\Delta t} \times \frac{1}{l} \beta(\psi^n) \delta_{IJ} d\Omega \cdot \psi_J^n = \oint_L -q_n N_I dL + \sum_e \int_{\Omega_e} Q N_I d\Omega + \sum_e \int_{\Omega_e} \frac{\overline{C}(\psi^n)}{\Delta t} \times \frac{1}{l} \beta(\psi^{n-1}) \delta_{IJ} d\Omega \cdot \psi_J^{n-1} \quad (20)$$

The above equation can be written as

$$[K_{IJ}(\psi) + O_{IJ}(\psi)] \cdot \psi_J^n = F_I(\psi) + \widetilde{O}_{IJ}(\psi) \cdot \psi_J^{n-1} - K_{IJ}(\psi) \cdot z_J \quad (21)$$

where

$$K_{IJ}(\psi) = \sum_e \int_{\Omega_e} N_{I,i} k_r(\psi^{n,m-1}) K_{ij} N_{J,j} d\Omega \quad (22)$$

$$O_{IJ}(\psi) = \sum_e \int_{\Omega_e} \frac{1}{l} \frac{\overline{C}(\psi^{n,m-1})}{\Delta t} \beta(\psi^{n,m-1}) \delta_{IJ} d\Omega \quad (23)$$

$$\widetilde{O}_{IJ}(\psi) = \sum_e \int_{\Omega_e} \frac{1}{l} \frac{\overline{C}(\psi^{n,m-1})}{\Delta t} \beta(\psi^{n-1}) \delta_{IJ} d\Omega \quad (24)$$

$$F_I(\psi) = \oint_L -q_n N_I dL + \sum_e \int_{\Omega_e} Q N_I d\Omega \quad (25)$$

Eq. (21) is the multi-dimensional finite-element algorithm in combination with the fully implicit standard Picard iteration for approximating the Richards' equation.

5. Boundary conditions

Dirichlet, Neumann, and seepage-face boundaries are considered. Dirichlet nodes, where the pressure heads are known, are described by

$$\psi_I = {}^{\dagger}\psi_I \quad (26)$$

where ${}^{\dagger}\psi_I$ are the known pressure heads at node I. The Ith equation in Eq. (21) is substituted by Eq. (26) directly.

Neumann boundaries which are named as flux boundaries are also treated in Eq. (21). If the soil of the elements related to a flux boundary is unsaturated and extremely dry, and the flux is relatively larger than the moisture conductivity, convergence difficulties may arise. Under these situations, the conductivity of the elements related to the boundary nodes is small and unable to quickly transmit the water away from the boundary node, resulting in a very large hydraulic gradient and unphysical surface pressure head bounds. The way to alleviate this problem is to provide a proper feedback in the matrix to the flux to keep the result within the physical bounds (Zhang et al., 2002). The convergence problem is solved but error may occur when the simulated percolating flux is less than the actual flux. This error can be reduced by the use of a thin layer of boundary elements.

A seepage face is an external boundary of the saturated zone where water leaves the soil and ψ is uniformly zero (namely, the pressure head equal to the surrounding air pressure). When the face is known a priori, the nodes inside the face are treated as Dirichlet nodes with the prescribed zero pressure head, while nodes outside the seepage face are specified as zero-flux nodes. Since the concrete position of seepage face is unknown a priori, the final location of the seepage face is determined by the flux of the node

$$Q_I = -K_{IJ} \cdot (\psi + z)_J \quad (27)$$

where Q_I is the flux at node I which may or may not be on the seepage face which is characterized by $\psi = 0$. If $Q_I > 0$, node I can be classified as a node on the seepage face, otherwise, it is classified as zero-flux boundary node (Wu and Gao, 1999).

6. Discussion on conductivity over a time-step

It does not need to get an average conductivity of an element in finite element methods, since the integral calculation of matrix in Eq. (11) by the gauss numerical integral method use the conductivity values of gauss points directly. However, values of hydraulic conductivity were evaluated at the half-time level other than at the nth time level by some researchers (Huang et al., 1994), namely, some kind of average of hydraulic conductivity may be considered over a time-step.

There are several kinds of average of hydraulic conductivity (e.g., arithmetic or geometric averages, explicit, fully implicit schemes, etc.) over space in the finite difference method (Zaidel and Russo, 1992). Having examined many other expressions for space (interblock) conductivity in the finite difference method, Haverkamp and Vauclin (1979) concluded that the geometric mean of k_i and $k_{i+1}, k_{i+1/2} = \sqrt{k_i k_{i+1}}$, is the best estimation of $k_{i+1/2}$. The relative conductivity over a time-step can also be geometric average, explicit, fully implicit.

The average relative permeability over a time-step $[t^{n-1}, t^n]$ in finite element method can be approximated as $k_r(\psi) = \sqrt{k_r(\psi^n) \cdot k_r(\psi^{n-1})}$ (geometric average), $k_r(\psi^{n-1})$ (explicit) or $k_r(\psi^n)$ (fully implicit). Which scheme is the best one will be discussed later in examples.

7. Algorithm validation and schemes comparison

The performance of the algorithm is compared with three illustrative sets of published experimental data, each of which represents a different physical scenario and is often used to validate algorithms. In the first example, the accuracy, mass balance character and iteration efficiency of the modified head based scheme (MHB) is compared with the modified Picard iteration scheme (MPI) using different time-step sizes, and the method of relative conductivity is also compared.

The parameters used in these numerical simulations are given in Table 1.

Table 1
Simulation parameters for Examples 1–3.

Example no.	θ_r	θ_s	α (1/m)	n	K_s (m/h)
1	0.15	0.38	1.66	2.62	0.016
2	0.01	0.30	3.3	4.1	0.35
3	0.01	0.30	3.3	4.1	0.40

7.1. Example 1: one-dimensional infiltration into a dry soil

The first test problem relates to a field example of variably saturated infiltration and solute transportation which was completed by Warrick et al. (1971). Although this problem is a one-dimensional infiltration process, the solution is achieved by using a two-dimensional mesh with no-flow boundaries imposed upon both vertical sides of the mesh to reproduce the one-dimensional conditions. Using one-dimensional problems to verify higher dimensional algorithms is a common strategy, as adopted by Van Genuchten (1982), Simpson and Clement (2003), and many others for validating their algorithms.

The soil is classified as Panoche clay loam. A 6.1- by 6.1 m plot had initially an approximately linear soil moisture content profile from 0.15 at the surface to 0.20 at the depth 0.6 m below the surface, and kept the value of 0.20 downwards. The plot was first wetted with 0.0762 m of 0.2 N $CaCl_2$ in 2.8 h, followed immediately by 0.229 m of solute-free water, and the infiltration lasted 17.5 h in total. The total infiltration water amounts to 0.3052 m. Tensiometers had previously been installed in duplicate at 0.3, 0.6, 0.9, 1.2,

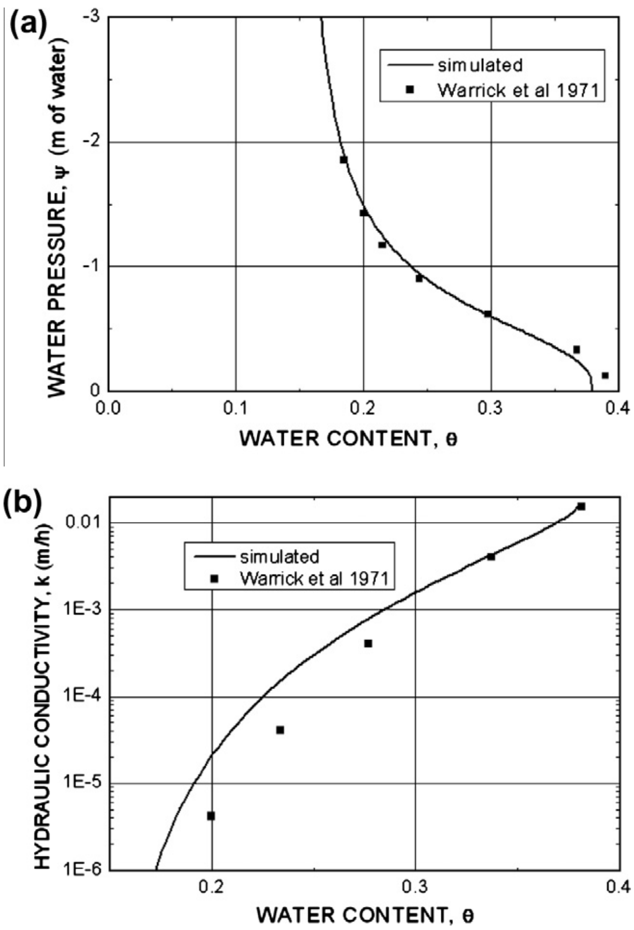

Fig. 1. Experimental (a) capillary saturation and (b) hydraulic conductivity data fitted by the van Genuchten and the Mualem functions.

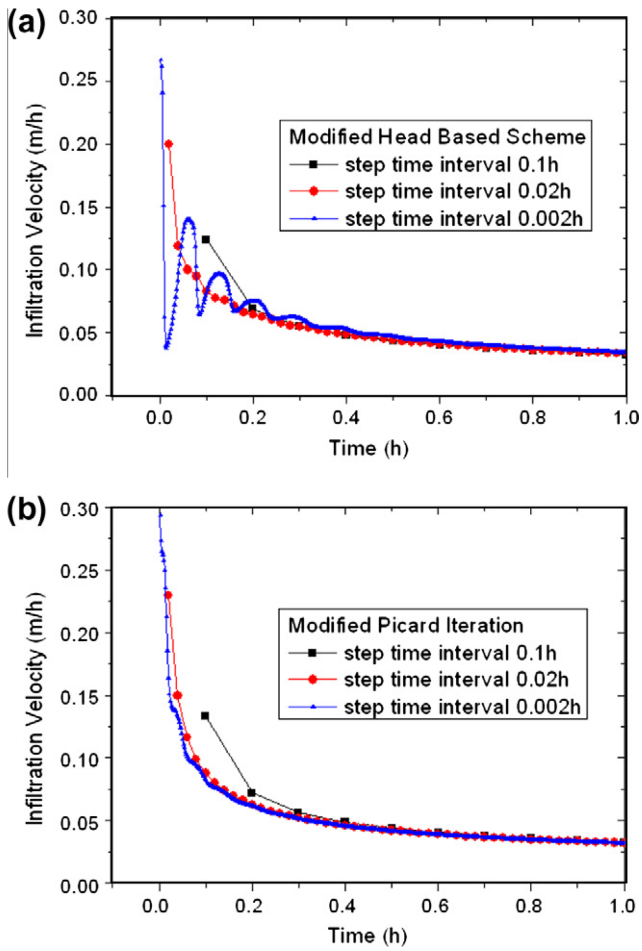

Fig. 2. Infiltration velocity at the soil surface using (a) modified head based scheme or (b) modified Picard.

1.5, and 1.8 m below the surface to monitor the water pressure head.

The average saturated moisture content of the soil is 0.38 and the saturated permeability is 0.0164 m/h. The hydraulic conductivity and pressure head vs. water content data are fitted by the soil characteristic functions as shown in Fig. 1a and b respectively, and the soil parameters are listed in Table 1. The 2 m depth of soil is meshed into 100 two-dimensional quadrilateral elements with a height of 0.02 m. The convergence criterion for the Picard iteration is that the largest pressure head error between two consecutive iteration steps should be less than 0.0001 m. The initial pressure head is calculated by the VG function. They are −100 m at the soil surface and vary from −18.4 m to −1.49 m at the nodes below. As for boundary conditions, the pressure head at the surface and at the bottom are 0 m and −1.49 m respectively.

The MHB scheme with the fully implicit conductivity method is first compared with the MPI scheme, and then geometric average and explicit conductivity method are compared with the fully implicit method based on the MHB scheme. Fig. 3 shows the curves of simulated infiltration velocity vs. time in the case of (a) MHB scheme and (b) MPI scheme at step-time sizes 0.002 h, 0.02 h and 0.1 h. These curves with different step-time sizes almost coincide after the initial 0.3 h in both the MHB and MPI schemes. In the MHB scheme the infiltration velocities fluctuate with time in the initial 0.3 h in the case of 0.002 h time-step size, but in the MPI scheme it does not. It is obvious that the hydraulic gradients of soil above the infiltration front decline with time since the influence of suction to the hydraulic gradients declines with the infiltration depth. The infiltration velocities in the case of 0.002 h time-step size in the MPI scheme is the most accurate simulation result; where the total infiltration mass is 0.3664 m. Table 2 shows the simulated total water infiltration mass and their error (in bracket) in comparison with the above-mentioned value. The differences of infiltration mass in these cases are small with the largest error up to 1.61%. Fig. 3 shows the variations of total water mass infiltration vs. time, revealing that the step-time size has little influence on the simulated infiltration mass both in the MHB and MPI schemes.

In Fig. 4a and b there are the curves of total mass balance ratio vs. time given by the MHB schemes and the MPI schemes, respectively. The values of total mass balance ratio of each curve both in Fig. 4a and b draw close to 1.0 with time. The time-step size has an obvious influence on the total mass balance ratio in the MHB schemes, but it has little influence in the MPI schemes. The mass balance character is good in the MHB scheme, it is better in the MPI scheme.

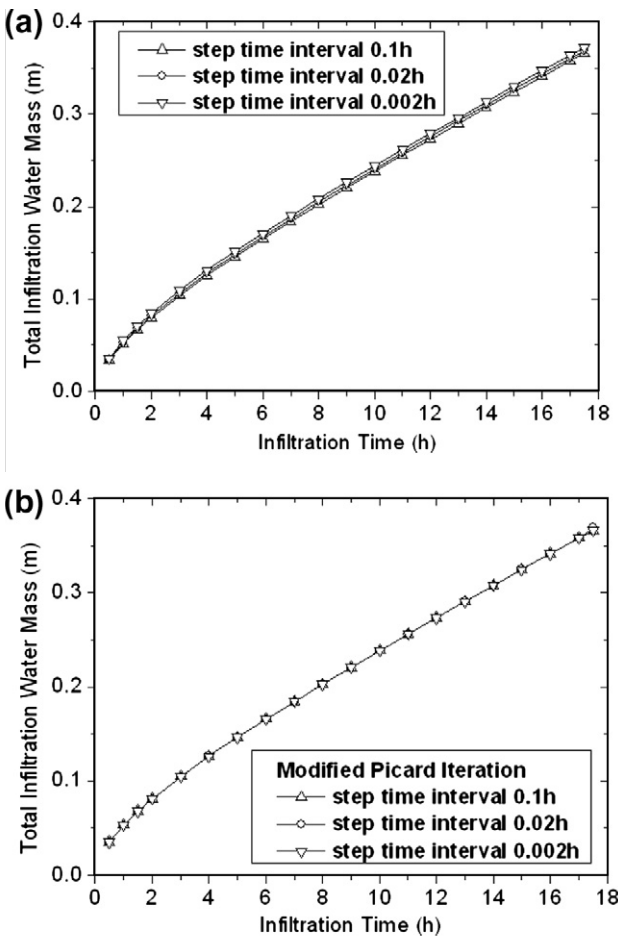

Fig. 3. Total water mass infiltration using (a) modified head based scheme or (b) modified Picard Iteration.

Table 2
Total simulated water infiltration (m) of schemes and error (in bracket) with fully implicit method.

Δt_n(h)	Modified Picard iteration	Modified head based scheme
0.002	0.3664	0.3723 (1.61%)
0.02	0.3665 (0.03%)	0.3689 (0.68%)
0.1	0.3666 (0.05%)	0.3659 (−0.14%)

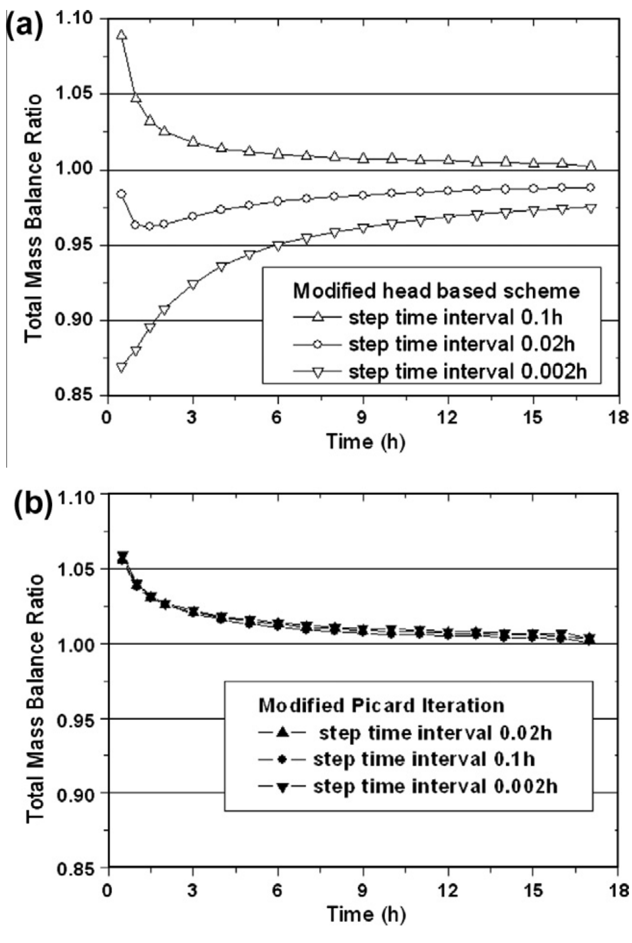

Fig. 4. Total mass balance ratio using (a) modified head based scheme or (b) modified Picard Iteration.

Fig. 5 is the number of iterations for achiving convergence when (a) MHB scheme or (b) MPI scheme is used. Curves of the iteration number decreases with the time-step size in MHB scheme, e.g. the less the time-step size, the less the number of iterations. This is a very important character, since the iteration efficiency can be improved by reducing the time-step size when a convergent problem occurs. The curves with 0.02 h and 0.002 h time-step size in MPI scheme fluctuate with time; the number of iterations at the first time-step in the case of 0.002 h is large. The number of iterations required in MHB is much less than that in MPI scheme in both the cases of 0.002 h and 0.02 h time-step sizes, but it is a little more in the case of 0.1 h time-step size. The iteration efficiency of MHB scheme is superior to that of MPI scheme.

The water infiltration velocity at the beginning point in this pond infiltration problem is infinity theoretically, it is between 0.125 and 0.3 m/h at the first step in the simulation cases as showed if Fig. 2, and it is 0.0167 m/h at 17.5 h, 1.04 times of the saturated conductivity of the soil, indicating that the hydraulic gradients behind the infiltration front are very large at the beginning due to the effect of suction. The infiltration velocity declines very quickly in the initial 0.1 h, and then decreases gradually and will finally approaches the saturated conductivity as the infiltration depth increases. For the infiltration problem a small time-step size should be adopted in the initial infiltration stage and a much larger step-time size can be used in the following stage to speedup the simulation process.

Fig. 6 shows the curves of simulated infiltration velocities vs. time for (a) explicit conductivity method and (b) geometric average conductivity method with the time-step sizes of 0.002 h, 0.02 h and 0.1 h. The simulated infiltration velocities in the explicit method are less than those given by the geometric average method in the initial stage, and both of them are less than those given by the fully implicit method which is considered as more reasonable. The comparison shows that the explicit and the geometric average methods are inferior in accuracy to the fully implicit method for pond infiltration problems. Fig. 7 is the number of iterations for achieving convergence when (a) the explicit method or (b) the geometric average method is used, showing that both methods have good iteration efficiencies. Table 3 lists the simulated total water infiltration masses given by them together with corresponding errors (in bracket) in comparison with 0.3664 m obtained from the fully implicit method. The explicit method with a large time-step size has large error. The fully implicit method is superior in accuracy and a large time-step size can be used, but its iteration efficiency is inferior to the other two. The fully implicit method is the first choice unless convergent problem appears.

The result of pressure head has been switched to moisture content via the VG function. The MBH simulated and experimental moisture content data at some time-steps are plotted in Fig. 8a. A sharp infiltration front propagating through the soil is obtained in the simulation, which resembles well the experimental results. The simulated total water intake is 20.1% larger than the test data, and thus the positions of the simulated infiltration front are much lower than the observed. If the saturated conductivity decreases to 0.0126 m/h, the total infiltration water would be 0.3065 m, 0.4% larger than the test value. The simulation results of moisture

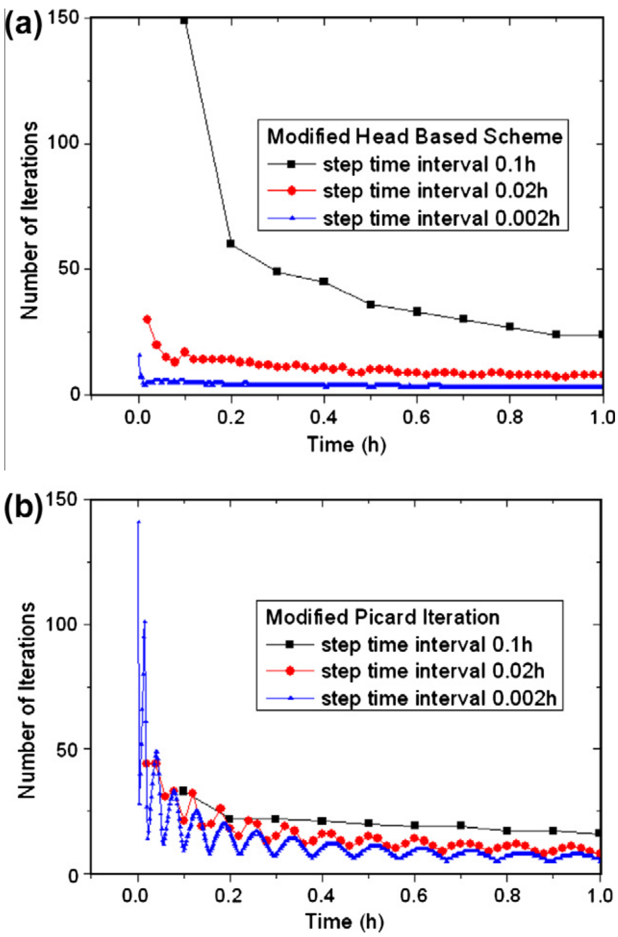

Fig. 5. Number of iterations required using (a) modified head based scheme or (b) modified Picard iteration.

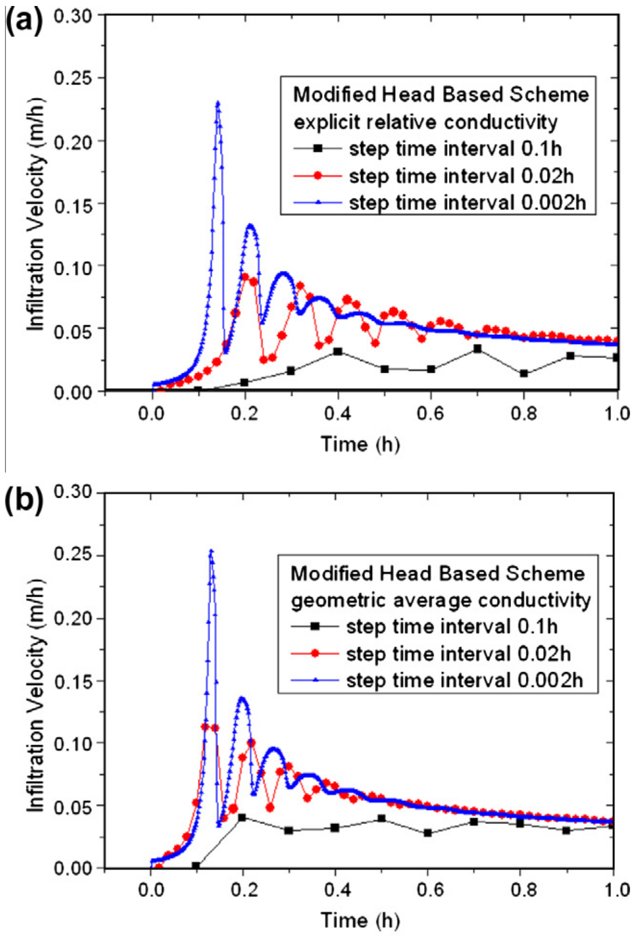

Fig. 6. Infiltration velocity at the soil surface using (a) explicit relative conductivity or (b) geometric average relative conductivity.

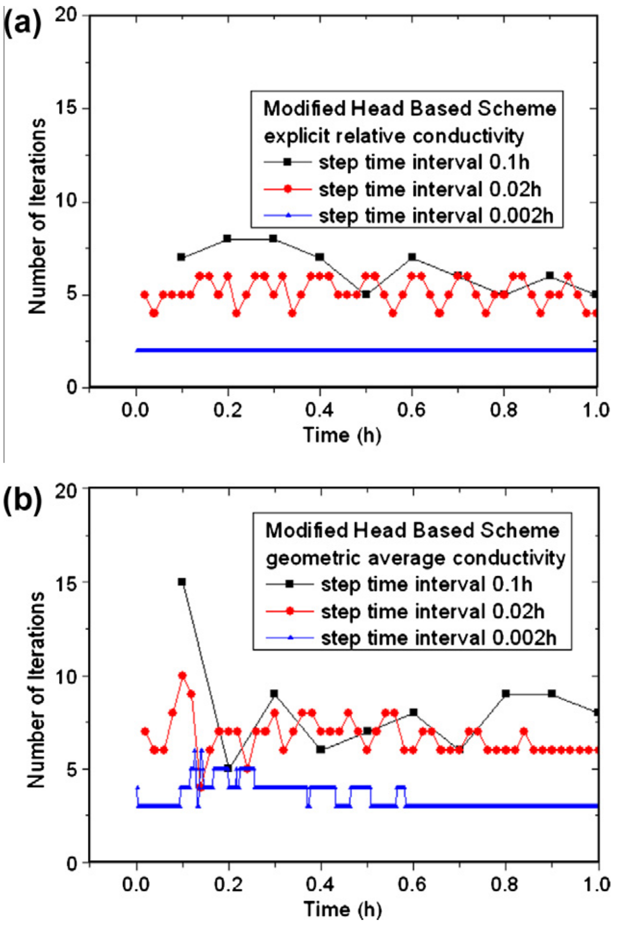

Fig. 7. Number of iterations required using (a) explicit relative conductivity or (b) geometric average relative conductivity.

Table 3
Total simulated water infiltration (m) of schemes and error (in bracket) with explicit conductivity and geometric average method.

Δt_n(h)	Explicit conductivity	Geometric average conductivity
0.002	0.3770 (2.89%)	0.3757 (2.54%)
0.02	0.3695 (0.85%)	0.3728 (1.75%)
0.1	0.3386 (−7.59%)	0.3547 (−3.19%)

content under this condition are plotted in Fig. 8b, they fit the test data well.

7.2. Example 2: two-dimensional transient variably saturated water table recharge

Experiments by Vauclin et al. (1979) were carried out in the laboratory on a slab of soil 6 m long, 2 m high, and 5 cm thick with an initial horizontal water table located at a height of 0.65 m. The bottom of the slab is impervious and its sides are drainage free. At the soil surface, a constant flux of $q = 0.148$ m/h was applied over a width of 1.00 m in the center region for 8 h, with the remaining soil surface covered to prevent evaporation losses. The soil is river sand of fairly regular grain-size distribution with 50% in weight passing through a mesh of 0.3 mm. The saturated moisture content and hydraulic conductivity are 0.3 and 0.35 m/h respectively. The moisture content and water pressure occurring in the flow domain were measured throughout the recharge event. These test data were often selected to verify the performance of algorithms for two dimensional transient variably saturated flows (Clement et al., 1994; Simpson and Clement, 2003). Parameters of the Van Genuchten function were fitted by Clement et al. (1994) and are given in Table 1. Fig. 9 shows the comparison of the measured soil water character curves and the values simulated by the van Genuchten and the Mualem functions.

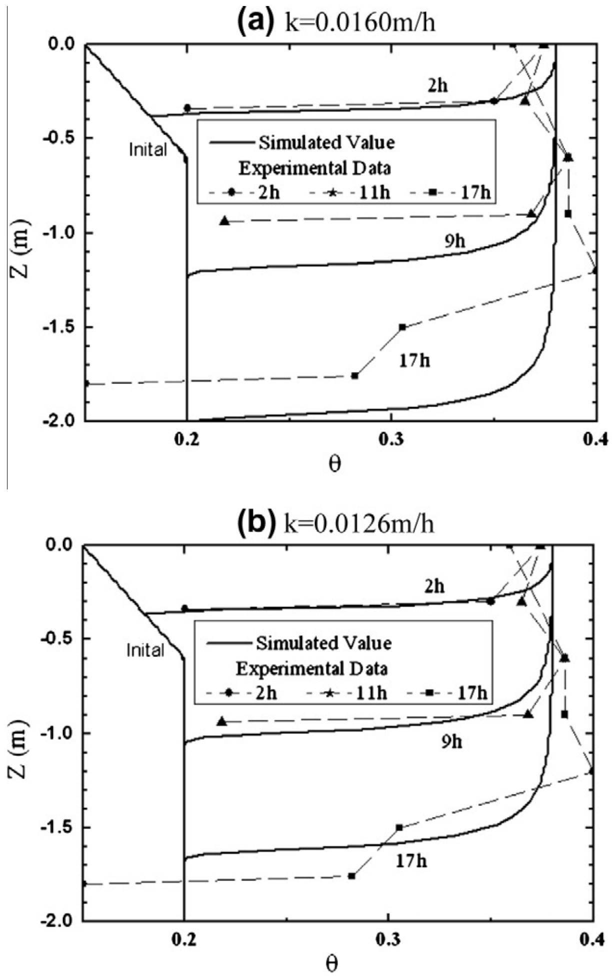

Fig. 8. Simulated and measured moisture content of a 1D field infiltration test (Warrick et al., 1971).

Because of the symmetry, only the right half flow domain is modeled. Total of 930 quadrilateral elements with a length of 10 cm and a height of about 6.5 cm was used to mesh the domain, and the time-step size is 0.02 h. The convergence criterion for the Picard iteration is that the largest pressure head error between two consecutive iteration steps should be less than 0.0001 m. The iteration does not converge if the fully implicit method is used, even if the time-step size is reduced. It does not converge after 200 iterations at the second time-step in the geometric conductivity method, however, it converges after 11 iterations after halving the time-step size. The time-step size increases by 20% at the following steps till it reaches 0.02 h again. The following iteration number for achieving convergence is between 2 and 12. The measured (Vauclin et al., 1975) and the simulated water table positions at different time-steps are plotted in Fig. 10. The root of the average square distance of the measured data points in Fig. 10 to the simulated curves is 19 mm, showing good agreement of the simulation results with the observations. Fig. 11 presents the contours of pressure head (m) calculated at time (a) 2 h, (b) 8 h after the start of infiltration, which are smooth everywhere including areas near the water table, indicating that there is no numerical oscillation.

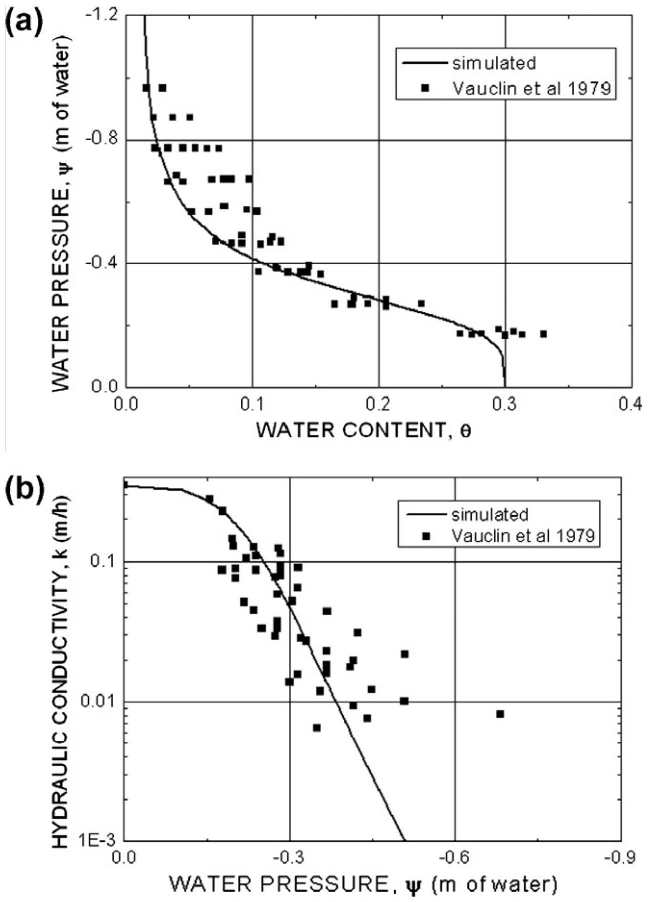

Fig. 9. Experimental (a) capillary pressure and (b) hydraulic conductivity data fitted with the van Genuchten and the Mualem functions.

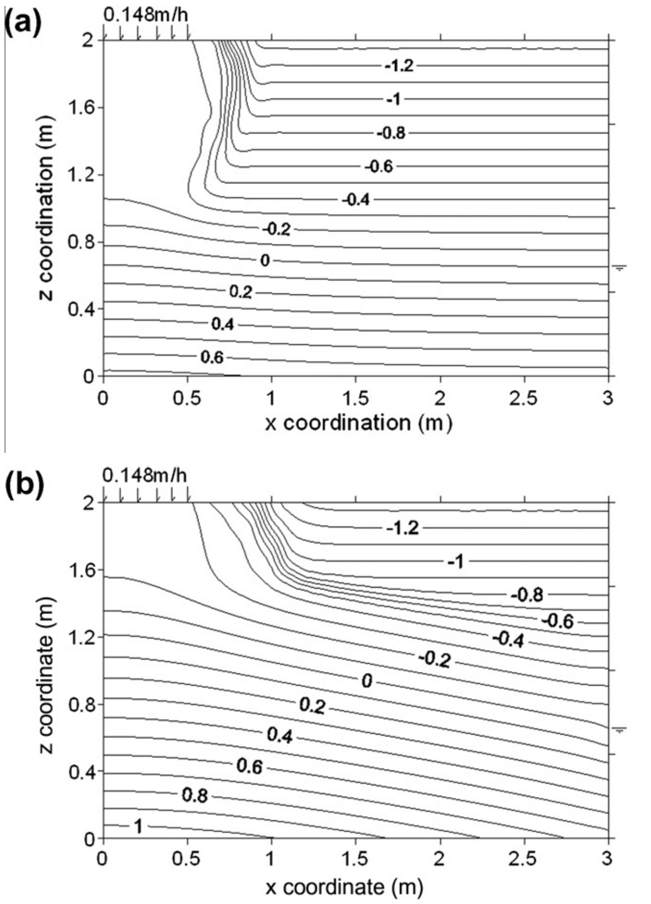

Fig. 11. Pressure head (m) calculated at time (a) 2 h, (b) 8 h after the start of infiltration.

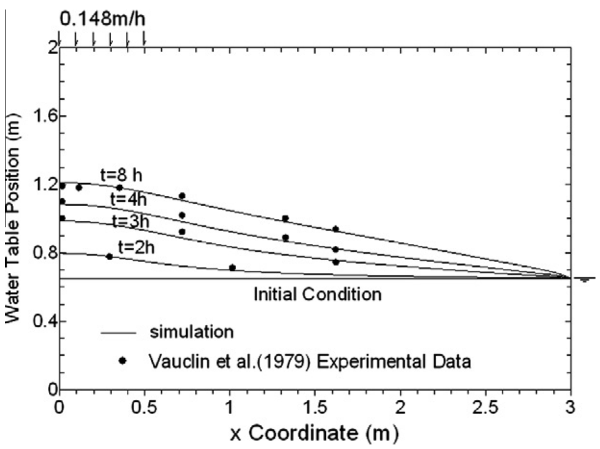

Fig. 10. Measured and simulated water table positions at different time.

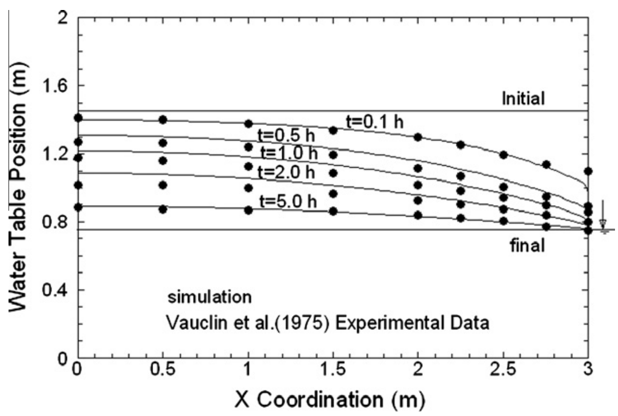

Fig. 12. Measured and simulated water table positions at different times in a transient drainage test.

7.3. Example 3: two-dimensional transient unconfined drainage

This example is chosen to validate the algorithm in modeling transient, unconfined drainage problems with seepage-face boundaries. Clement et al. (1994) presented an experiment performed by Vauclin et al. (1975) on the transient locations of seepage face and water table in a two-dimensional drainage problem. The device used in this test is the same as used in Example 2. A 6.00×2.00 m saturated porous medium was allowed to drain after a sudden drop in the external water table. Moisture contents and pressure heads were measured during the entire transient drainage phase until the steady-state conditions were reached. The initial water table was kept at 1.45 m. At time $t = 0$, the external water table was dropped to the height of 0.75 m, and was maintained there subsequently. Owing to the symmetry of this problem, the right half is used for simulation as did in Example 2 with the same mesh. The half domain has no-flux boundaries on the bottom, top, and the left side (according to the symmetric condition). Since the temporal location of the seepage face at a given time is unknown until the problem is solved, the seepage-face boundary between 0.75 and 1.45 at the right side is determined by the seepage face treatment method described in Section 5.

All the parameters are the same as used in Example 2 and shown in Table 1. The constant time-step size is 0.02 h and the convergence criterion for the Picard iteration is that the largest pressure head error between two consecutive iteration steps should be less than 0.0001 m. In the fully implicit method, it does not converge after 200 iterations at time 1.02 h, however, it converges after halving the time-step size to 0.01 h, the time-step size increases by 20% at the following steps till it reaches 0.02 h again. In the following computation, convergence is achieved after 5–19 iterations. In the geometric average method, the iteration numbers for achieving convergence are between 5 and 7 with a constant time-step size of 0.02 h. The simulated water table positions are the same in these two schemes, and it is compared in Fig. 12 with the experimental results given by Vauclin et al. (1975). The root of the average square distance of the measured data points to the simulated curves is 28.5 mm, indicating that the proposed model is capable of reproducing closely the experimental results.

8. Conclusion

An algorithm is presented to solve the Richards' equation for multi-dimensional flow problems in variably saturated soils. In particular, the problem of mass-balance errors is tackled, which is indeed a pressing problem for the simulation of such highly nonlinear phenomena as the infiltration in a dry soil. The effectiveness of the algorithm is demonstrated by comparison with published data sets. A modified head based method proposed by the author and the modified Picard iteration method are compared in the one-dimensional field infiltration example, where three step-time sizes are adopted and compared too. Both methods are mass-conservative and efficient in iteration; the MBH method is a little inferior in respect of mass balance, but is superior in convergence character and iteration efficiency. Generally, large time-step size requires large iteration number to converge, however, the time-step size has little influence on simulation accuracy in the fully implicit conductivity method. Hence large time-step size can be used to speedup simulation process. Explicit and geometric average conductivity have good iteration efficiency but they are inferior in accuracy in ponding infiltration problems. The geometric average method can be used when convergence problem occurs in applying the fully implicit method. The algorithm is demonstrated to work well for the problems of infiltration fronts, steady-state and transient water tables as well as transient seepage faces.

The success of the algorithm in simulating a variety of problems leads to confidence in its applicability to many variably saturated flow problems. The finite element method is still superior to other numerical methods in simulating transient flows for its advantageous flexibility suited to complicated inner and exterior boundaries.

Acknowledgments

This work was supported partially by the Natural Science Foundation of China (Grant No. 10932012), by Chinese Academy of Sciences (No. KJCX2-YW-L02), by the Ministry of Science and Technology of China (No. 0820), and by European Commission (No. FP7-NMP-2007-LARGE-1). However, it has not been submitted to the agency's administrative and peer review. Therefore, it does not necessarily reflect the agency's views and no official endorsement should be inferred.

References

Celia, M.A., Efthimios, T.B., Rebecca, L.Z., 1990. A general mass-conservative numerical solution for the unsaturated flow equation. Water Resources Research 26 (8), 1483–1496.

Clement, T.P., Wise, W.R., Molz, F.J., 1994. A physically based, two-dimensional, finite- difference algorithm for modeling variably saturated flow. Journal of Hydrology 161, 71–90.

Hao, X., Zhang, R., Kravchenko, A., 2005. A mass-conservative switching method for simulating saturated–unsaturated flow. Journal of Hydrology 311, 254–265.

Huang, K., Mohanty, B.P., van Genuchten, M.Th., 1996. A new convergence criterion for the modified Picard iteration method to solve the variably saturated flow equation. Journal of Hydrology 178, 69–91.

Huang, K., Zhang, R., van Genuchten, M.Th., 1994. An Eulerian–Lagrangian approach with an adaptively corrected method of characteristics to simulate. Water Resource Research 30 (2), 499–507.

Haverkamp, R., Vauclin, M., 1979. A note on estimating finite difference interblock hydraulic conductivity values for transient unsaturated flow problems. Water Resource Research 15, 181–187.

Kavetski, D., Binning, P., Sloan, S.W., 2001. Adaptive time stepping and error control in a mass conservative numerical solution of the mixed form of Richards' equation. Advances in Water Resources 24, 595–605.

Mcbride, D., Cross, M., Croft, N., Bennett, C., Gebhardt, J., 2005. Computational modeling of variably saturated flow in porous media with complex three-dimensional geometries. International Journal for Numerical Methods in Fluids, Published online in Wiley InterScience. <www.wiley.com>. doi:10.1002/Fld.1087.

Milly, P.C.D., 1985. A mass-conservative procedure for time-stepping in nodes of unsaturated flow. Advances Water Resources 8, 32–36.

Mualem, Y., 1976. A new model for predicting the conductivity of unsaturated porous media. Water Resources 12, 513–522.

Neuman, S.P., 1999. Saturated–unsaturated flow seepage by finite element. Proc. ASCE, Journal of the Hydraulic Division 99 (HY12).

Richards, L.A., 1931. Capillary conduction of liquids through porous mediums. Physics 1, 318–333.

Simpson, M.J., Clement, T.P., 2003. Comparison of finite difference and finite element solutions to the variably saturated flow equation. Journal of Hydrology 270, 49–64.

Van Genuchten, M.Th., 1980. A closed-form equation for predicting the hydraulic conductivity of unsaturated soils. Soil Science of American Journal 44, 892–898.

Van Genuchten, M.Th., 1982. A comparison of numerical solutions of the one-dimensional unsaturated-saturated flow and mass transport equations. Advances in Water Resources 5 (1), 47–55.

Vauclin, M., Khanji, D., Vauchaud, G., 1979. Experimental and numerical study of a transient two-dimensional unsaturated–saturated water table problem. Water Resources Research 15 (5), 1089–1101.

Vauclin, M., Vachaud, G., Khanji, J., 1975. Two dimension numerical analysis of transient water transfer in saturated–unsaturated soils. In: Vansteenkiste, G.C. (Ed.), Modeling and Simulation of Water Resources Systems. North-holland, Amsterdam, pp. 299–323.

Warrick, A.W., Biggar, J.W., Nielsen, D.R., 1971. Simultaneous solute and water transfer for an unsaturated soil. Water Resources Research 7 (5), 1216–1225.

Wu, Mengxi, Gao, Lianshi, 1999. Numerical simulation of saturated–unsaturated transient flow in soils. Journal of Hydraulic Engineering 1999 (12), 38–42.

Zhang, X.X., Glyn Bengough, A., Crawford, J.W., Young, I.M., 2002. Efficient methods for solving water flow in variably saturated soils under prescribed flux infiltration. Journal of Hydrology 260 (2002), 75–87.

Zaidel, J., Russo, D., 1992. Estimation of finite difference interblock conductivities for simulation of infiltration into initially dry soils. Water Resources Research 28 (9), 2285–2295.